ACS APPLIED MATERIALS & INTERFACES

Research Article

www.acsami.org

Fully Solution-Processed Transparent Conducting Oxide-Free Counter Electrodes for Dye-Sensitized Solar Cells: Spray-Coated Single-Wall Carbon Nanotube Thin Films Loaded with Chemically-Reduced Platinum Nanoparticles

Sang Yong Kim,[†] Yesel Kim,[†] Kyung Moon Lee,[†] Woo Sug Yoon,[‡] Ho Seok Lee,[‡] Jong Tae Lee,[‡] Seung-Joo Kim,[†] Yeong Hwan Ahn,[†] Ji-Yong Park,[†] Tai Kyu Lee,[‡] and Soonil Lee*[,†]

[†]Department of Physics and Division of Energy Systems Research, Ajou University, Suwon 443-749, Korea

[‡]NANOPAC, Yongin, 449-832, Korea

Supporting Information

ABSTRACT: We report fully solution-processed fabrication of transparent conducting oxide-free counter electrodes (CEs) for dye-sensitized solar cells (DSSCs) by combining spray-coating of single-wall carbon nanotubes (SWCNTs) and chemical reduction of chloroplatinic acid precursor to platinum nanoparticles (Pt NPs) with formic acid. The power conversion efficiency of a semitransparent DSSC with such SWCNT-based CE loaded with Pt NPs is comparable to that of a control device with a conventional CE. Quantification of Pt loading shows that network morphology of entangled SWCNTs is efficient in forming and retaining chemically reduced Pt NPs. Moreover, electron microscopy and electrochemical impedance spectroscopy results show that mainly Pt NPs, which are tens of nanometers in diameter and reside at the surface of SWCNT CEs, contribute to electrocatalytic activity for triiodide reduction, to which we attribute strong correlation between power conversion efficiency of DSSCs and time constant deduced from equivalent-circuit analysis of impedance spectra.

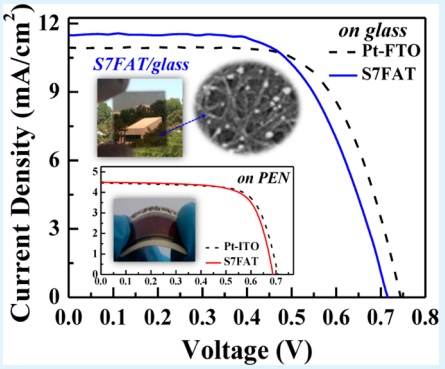

KEYWORDS: *transparent conducting electrode, single-wall carbon nanotube, chemical reduction, full solution processability, semitransparent DSSC*

1. INTRODUCTION

Dye-sensitized solar cells (DSSCs) have attracted large scientific and industrial interest as a viable option for practical applications because of their simple structure, low production cost, and high power conversion efficiency (PCE).[1] However, similar to the cases of other thin film solar cells,[2,3] the development of flexible DSSCs that can greatly accelerate the commercialization of DSSCs remains a challenge. Fabrication of key elements of DSSCs based on solution processes is important, in particular, to reduce the manufacturing cost further and to utilize common electronics-grade plastic films.

In this work, we developed an alternative counter electrode (CE) based on single-wall carbon nanotubes (SWCNTs) that can replace conventional transparent conducting oxide (TCO) electrodes, such as fluorine-doped tin oxide (FTO) and indium-doped tin oxide (ITO). ITO-coated plastic films decorated with vacuum-deposited platinum nanoparticles (Pt NPs) have been studied as typical CEs for flexible DSSCs.[4] However, the viability of such ITO-based CEs for flexible DSSCs is limited by several drawbacks including high material and processing cost, and its tendency to crack upon flexion. Carbon materials such as activated charcoal, carbon black, carbon nanotubes (CNTs), carbon nanofibers, and graphene have been studied to develop inexpensive CEs by taking advantage of their electrocatalytic capacity for triiodide reduction.[5−9] In particular, CNTs have been widely studied because of their excellent electrical conductivity, chemical inertness, and high catalytic activity.[10] Various deposition methods such as spraying, electrophoresis, doctor blading, screen printing, and vertical growth have been used to make CNT CEs having triiodide-reduction capacity comparable to that of conventional Pt-TCO CEs.[11−15] However, fabrication of Pt-free CNT CEs require the formation of thick CNT films with a thickness ranging from several to tens of μm[16] similar to other carbon material cases. We note that carbon-material CEs with such thicknesses cannot be compatible with semitransparent DSSCs and are susceptible to cracking and/or detachment from its plastic substrates when devices are flexed. To address these issues, composite type CEs that combine carbon materials with Pt, conducting polymer, or metal nitride and sulfide are being actively studied.[4,17−20]

The most promising alternative CEs for flexible DSSCs is naturally the combination of CNTs and Pt NPs to take

Received: March 31, 2014
Accepted: August 7, 2014
Published: August 14, 2014

   dx.doi.org/10.1021/am5019447 | ACS Appl. Mater. Interfaces 2014, 6, 13430−13437

advantage of the high electrocatalytic activity of Pt NPs together with the excellent electrical and mechanical traits of CNTs.[21−23] Chen et al. used a two-step process that consisted of decorating CNTs with Pt NPs using an ionic liquid-assisted sonochemical method and subsequently electrospinning the Pt NP-decorated CNTs on TCOs to make CEs.[21] Alternatively, CEs can be fabricated directly through high-temperature treatment of Pt precursor-containing CNT-dispersed solution, paste, or slurry coated on TCOs.[24,25] Huang et al. reported an example of such CEs fabricated by annealing a composite solution of multiwall CNTs (MWCNTs), Pt precursor, poly(oxyethylene)-segmented imide polymer (POEM), and sodium borohydride ($NaBH_4$) spin-coated on FTO substrates at 390 °C for 20 min. POEM and $NaBH_4$ were used as a polymeric dispersant and a chemical reduction agent, respectively.[26] One problem closely related to the decoration of CNTs with Pt NPs is the degradation of the mechanical and electrical properties of CNTs resulting from its functionalization.[27] On the other hand, Lin et al. reported the fabrication of Pt-decorated MWCNT CEs through thermal treatment of a viscous dispersion mixture of unfunctionalized MWCNTs, POEM, and H_2PtCl_6 at 390 °C for 20 min.[28] The PCEs of their DSSCs with a TCO-free Pt-loaded MWCNT CE were comparable with those of Pt-loaded TCO CEs. However, the high processing temperature makes their method incompatible with plastic substrates.

One promising way to alleviate the problems associated with high processing temperature is to utilize a totally different method for Pt-NP formation. Recently, there was report of TCO-free CE fabrication using a spontaneous reduction method. In this approach, SWCNT films spray coated on TCO-free substrates were dipped into a 5 mM Na_2PtCl_4 precursor solution and then dried, to result in Pt-loaded SWCNT CEs.[29] The PCE of a DSSC with a Pt NP-SWCNT CE based on spontaneously reduction was only about 73% of that of a DSSC with a conventional Pt NP-FTO CE. Using chemical reductant such as $NaBH_4$[30] or formic acid (HCOOH)[31,32] is another way to convert Pt precursors to Pt NPs without high-temperature processing.

In this work we combined spray-coating of aqueous dispersion solution of SWCNTs, which had been successfully used to fabricate TCEs for organic solar cells (OSCs) having PCE values comparable to those of conventional OSCs with an ITO TCE,[33] with chemical reduction of Pt precursor to fabricate fully solution-processed CEs. Because the solution processing was conducted entirely at low temperatures (<150 °C) our new CE-fabrication method that utilizes formic acid as a reduction agent is compatible with common electronics-grade plastic substrates, thereby lending potential for large-scale production at low cost.

2. EXPERIMENTAL SECTION

To prepare an aqueous dispersion solution for spray coating, arc-made SWCNTs (SA210, Nano Solution Co.) were purified and dispersed in water by using sodium dodecyl benzenesulfonate (SDBS) as a surfactant. First, raw SWCNTs were stirred with ultrapure water (DV35, ELGA) to obtain a solution with concentration of 1 mg/mL, and then 0.3 wt % of SDBS was added to the SWCNT−water solution. Next, the SDBS−SWCNT aqueous solution was subjected to 600 W ultrasonication at 38 kHz (SW 6H, Sonoswiss AG) for 2 h. Lastly, the solution was centrifuged for 15 min at 20 000 rpm (CR22G, Hitachi) twice to complete preparation of an aqueous dispersion solution of SWCNTs for spray coating.

SWCNT films were spray-coated on glass substrates, the surfaces of which were thoroughly cleaned and pretreated with (3-aminopropyl)-triethoxysilane (APTES) that is a coupling agent between SWCNTs and glass substrates. Pretreatment was done by immersing glass substrates in an aqueous bath of 1% APTES for 5 min. In the case of flexible CEs, SWCNT films were spray-coated on a piece of polyethylene naphthalate (PEN: Q65FA, Teijin Dupont) that was pretreated for 10 min in a UVO cleaner (AH-1700, AHTech LTS). During SWCNT spray-coating, the temperature of APTES-treated glass and PEN substrates were maintained at 100 °C on a hot plate. SWCNTs were uniformly coated by using a commercial spray gun with a nozzle size of 0.2 mm (Colani Airbrush, Harder and Steenbeck). Subsequently, SWCNT-coated substrates were dipped in a warm bath of ultrapure water at 50 °C for 1 h to remove SDBS. Additional treatment with nitric acid fume at 115 °C for 1 h was required for more thorough removal of SDBS. The final step in SWCNT-film coating was to bake it in a vacuum oven at 80 °C for 2 h to remove residual nitric acid.

The fabrication of a CE was completed through low-temperature chemical processing that used formic acid (HCOOH, 95%) as a reducing agent to transform chloroplatinic acid precursor into Pt NPs. A 30 mM precursor solution was prepared by dissolving chloroplatinic acid hydrate ($H_2PtCl_6{\cdot}nH_2O$, n = 5.8, Kojima Chemicals) in isopropyl alcohol. A 75 μL portion of the Pt-precursor solution was spin-coated on the SWCNT films at 1800 rpm for 20 s and then dried at 85 °C for 90 s on a hot plate. The chemical reduction process consisted of immersing Pt precursor-coated SWCNT electrodes in a 5% aqueous solution of formic acid, baking at 75 °C for 90 min in a convection oven, and rinsing with ultrapure water for 20 s to remove excessive formic acid and other residues. To vary Pt-NP loading in SWCNT CEs, the spin-coating of a Pt-precursor solution was repeated four and seven times prior to formic acid treatment (FAT).

A conventional recipe was followed to prepare a TiO_2 photoanode. At first, an 8 Ω/sq FTO-coated glass substrate (TEC-8, Pikington) was thoroughly cleaned and pretreated with $TiCl_4$. The treatment process consisted of immersing the substrate in a 40 mM aqueous solution of $TiCl_4$, baking at 70 °C for 30 min, rinsing with ultrapure water and ethanol, and annealing at 500 °C for 30 min. Next, TiO_2 paste (18NR-T, Dyesol) was coated onto $TiCl_4$-pretreated FTO glasses by using a doctor-blade method, dried at 50 and 70 °C for 15 min each, and annealed at 525 °C for 40 min. Subsequently, the annealed TiO_2 photoanode was treated again with $TiCl_4$ by repeating the aforementioned process. Finally, the TiO_2 photoanode was loaded with dye (N719, Dyesol) at 75 °C for 8 h. Before dipping in a 0.3 mM ethanol solution of N719, the TiO_2 photoanode was dried by baking at 130 °C for 30 min.

A modified recipe was used to make a low-temperature photoanode for a flexible DSSC. After UV-ozone pretreatment of the surface of a piece of 15 Ω/sq ITO-coated PEN (PECF-IP, Peccell) for 10 min, a solution of TiO_2 NPs (diameter of ∼15 nm, 10 wt %) was spin-coated on the ITO-coated PEN at 1800 rpm for 40 s, dried in ambient air for 30 min, and then baked at 150 °C for 30 min in a convection oven. Next, a binder-free TiO_2 paste, which was prepared by mixing commercial TiO_2 NPs (P-25, Degussa) with a 2:1 (volume ratio) blend of Tert-Butanol and DI water for 3 d, was coated by doctor blading and baked at 150 °C for 30 min. A dye-loading process was identical with that of conventional high-temperature photoanodes.

Dye-loaded TiO_2 photoanodes and Pt NP-decorated SWCNT CEs were assembled and sealed with a 60 μm thick Surlyn tape (Meltonix 1170−60, Solaronix SA), and then iodide/triiodide-based liquid electrolyte (EL-HSE, Dyesol) was filled through a predrilled hole to complete DSSC fabrication. Finally, exterior contact electrodes were formed by using an ultrasonic solder (USS-9210, MBR Electronics) to secure a good electrical contact. The DSSC devices with a SWCNT CE loaded with FAT-formed Pt NPs are designated respectively as S1FAT, S4FAT, and S7FAT according to the Pt-precursor spin-coating number of 1, 4, and 7. Two other SWCNT-CE DSSCs were fabricated for comparison, one without FAT after a single spin coating of Pt precursor (S1NFT) and the other one without both Pt-precursor spin coating and FAT (S0NFT). As a control device, a conventional

DSSC having a Pt-FTO CE that was prepared through thermal reduction of spin-coated Pt precursor on a FTO glass at 400 °C for 20 min was also fabricated (PtFTO). In the case of flexible DSSCs, a 7 nm Pt layer was deposited on ITO/PEN by e-beam evaporation to make a CE for a control device.

Thickness and optical transmittance of both electrodes were measured with a stylus-type surface profiler (P-10, Tencor) and a UV−vis spectrophotometer (Cary 5000, Varian), respectively. Morphology and chemical composition of CEs were obtained using a field-emission scanning electron microscope (FESEM: S-4800, Hitachi), a scanning transmission electron microscope (STEM: JEM-2100F, Jeol), and an energy-dispersive X-ray spectroscopy (EDS) system operated at the acceleration voltage of 15 kV. Process-dependent variations in the sheet resistance of bare and Pt NP-loaded SWCNT CEs were monitored with an automatic four point probe system (model 280, Four Dimensions). Photovoltaic performance of DSSCs were measured under standard AM 1.5 sunlight condition by using a solar simulator (PEC-L01, Peccell) that was calibrated to 100 mW/cm^2 with a reference Si cell (PEC-S101, Peccell). For reliable assessment of DSSC operation a black mask was used for all measurements.[34] Electrochemical impedance spectroscopy (EIS) measurements were performed with a portable electrochemical interface and impedance analyzer system (CompactStat, Ivium Technologies) in the frequency range from 0.1 Hz to 100 kHz. Measured EIS spectra were analyzed based on equivalent circuit models through Z-view fitting.

3. RESULTS AND DISCUSSION

Figure 1a is a photograph of typical semitransparent DSSCs with a Pt NP-decorated SWCNT counter electrode. Optical

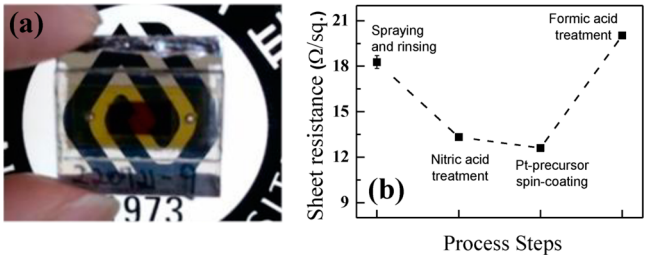

Figure 1. (a) A photograph of the device S7FAT, which is a typical image of DSSCs with a Pt NP-loaded SWCNT CE, and (b) the process-dependent variation of sheet resistance of a typical SWCNT CE.

transmittance of semitransparent DSSCs depends mostly on the transparency of spray-coated SWCNT films regardless of Pt precursor-coating number.

The use of SWCNT films having average thickness of 128 ± 8 nm made it possible to fabricate semitransparent DSSCs with optical transmittance of 25% at wavelength of 550 nm. The optical transmittance increased at longer wavelengths and became greater than 35% in the red and near IR spectral range (Supporting Information, Figure S1). However, the sheet resistance of such SWCNT films showed a process-dependent systematic variation as shown in Figure 1b. The measured sheet resistance that was initially 18.28 ± 0.43 Ω/sq right after the spraying and washing steps was reduced to 13.33 ± 0.23 Ω/sq following a nitric-acid fume treatment, but increased to the final value of 20.03 ± 0.05 Ω/sq following a subsequent formic-acid treatment. It seems the nitric-acid fume treatment for thorough surfactant removal resulted in SWCNT doping,[35] whereas the formic-acid treatment intended to reduce the Pt precursor induced SWCNT dedoping. Bleaching of absorption bands of semiconducting SWCNTs in transmittance (Supporting

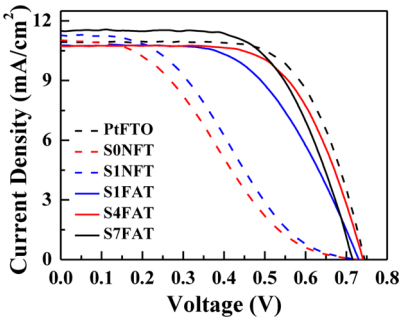

Figure 2. Comparison of photovoltaic performance of DSSCs with different types of CEs. Solid lines correspond to the DSSCs with SWCNT CE loaded with Pt NPs formed by using formic acid treatment; a Pt-precursor solution was spin-coated once (blue), four times (red), and seven times (black) on SWCNT film electrodes. The black dash line represents a control device with a conventional Pt-FTO CE, and the red dash line a device with a SWCNT-only CE. Another SWCNT CE device that was spin coated with a Pt-precursor solution without subsequent treatment with formic acid is represented by the blue dash line.

Information, Figure S1) and blue-shifts of G and G' Raman peaks (Supporting Information, Figure S2) of SWCNTs are evidence for anodic doping. Comparatively, the reappearance of disappeared absorption bands (Supporting Information, Figure S1) and red-shifts of G and G' peaks (Supporting Information, Figure S2) are clearly indicative of dedoping of SWCNTs.

Figure 2 shows typical current−voltage (I−V) characteristics of a series of DSSCs fabricated using different types of CEs. For reliable comparison of CE performance, we paid special attention to making all other parts of the DSSCs to be identical, and made three devices for each CE type. The average thickness and area of photoanodes were 13.0 ± 0.22 μm and 0.321 ± 0.10 cm^2, respectively. The I−V curves in Figure 2 were measured by using a black mask with an aperture area of 0.418 cm^2. We note that the two devices S0NFT and S1NFT show very poor performance compared to other devices with a SWCNT CE. In comparison performances of the other three SWCNT-CE devices are comparable with that of a control device with a conventional Pt-FTO CE. The poor performances of S0NFT and S1NFT indicate that thin SWCNT films do not possess sufficient reduction capacity to make catalytic Pt NPs dispensable, and that an active reduction process is required to form catalytic Pt NPs. On the other hand, the much improved performances of the three SWCNT-CE devices that were treated with formic acid after Pt-precursor spin-coating indicate that the low-temperature chemical reduction process relying on formic acid was efficient in producing catalytic Pt NPs. Moreover, the performance differences among these three SWCNT-CE devices suggest that Pt-NP loading of SWCNT electrodes was dependent on the details of Pt-precursor spin-coating.

The average values of important solar-cell parameters extracted from the I−V curves are summarized in Table 1. The control devices with a conventional Pt-FTO CE shows very typical parameter values, such as open-circuit voltage (V_{oc}) of 0.754 V, short-circuit current density (J_{sc}) of 10.8 mA/cm^2, fill factor (FF) of 66.9%, and, consequently, PCE of 5.42%. In accordance with the I−V curves in Figure 2, FF values of the two types of SWCNT-CE devices without Pt-catalyst loading (S0NFT and S1NFT) are markedly inferior to those of the control device and responsible for low PCEs, whereas V_{oc} and

Table 1. Average Values of Solar Cell Parameters Corresponding to Each Type of Counter Electrode

sample ID[a]	V_{oc} (V)	J_{sc} (mA/cm^2)	fill factor (%)	PCE (%)
PtFTO	0.754 ± 0.008	10.8 ± 0.20	66.9 ± 0.6	5.42 ± 0.01
S0NFT	0.726 ± 0.005	11.1 ± 0.05	30.4 ± 0.6	2.44 ± 0.04
S1NFT	0.729 ± 0.015	10.8 ± 0.53	35.2 ± 0.7	2.77 ± 0.04
S1FAT	0.737 ± 0.013	10.6 ± 0.35	58.6 ± 2.0	4.56 ± 0.13
S4FAT	0.743 ± 0.017	10.7 ± 0.27	63.8 ± 0.5	5.08 ± 0.02
S7FAT	0.720 ± 0.007	11.3 ± 0.17	62.8 ± 0.7	5.11 ± 0.07

[a]Average values are estimated from three devices of each type. Standard deviations of each parameter value are typically less than 3% of the average values.

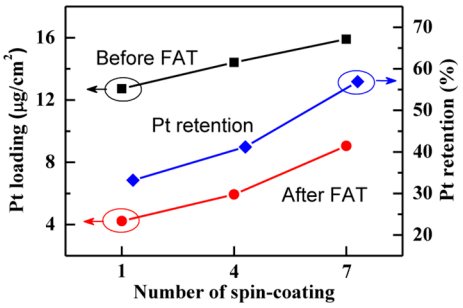

Figure 3. Initial amount of spin-coated Pt (■) increased monotonically with respect to precursor spin-coating repetitions. Both the Pt-NP loading after FAT (●) and the Pt-retention ratio (◆) that is the ratio between the amounts of Pt before and after FAT showed similar monotonic variations. The amounts of Pt were determined based on EDS measurements.

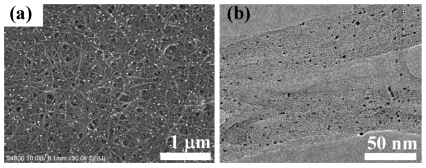

Figure 4. Typical SEM and TEM images of FAT-SWCNT CEs: The images in (a) and (b) correspond to S4FAT and S7FAT CEs, respectively. (a) The high-magnification SEM image shows that Pt NPs having tens of nanometers diameters were formed at the surface of a FAT-SWCNT CE. (b) The TEM image shows that the SWCNTs themselves were decorated with smaller Pt NPs with diameter of a few nanometers.

J_{sc} values are similar to those of the control device. Such dramatic FF degradation is a clear evidence of insufficient electrocatalytic activity for triiodide reduction of these thin SWCNT CEs.[11,16] A slightly larger PCE of the S1NFT indicates that even very limited conversion of precursor into Pt can be beneficial in enhancing the triiodide-reduction activity of a CE.

In the case of three FAT-SWCNT CEs, FF values are markedly improved while their V_{oc} and J_{sc} values remain close to those of the control devices. Correspondingly, PCEs of the three FAT-SWCNT CEs show substantial increases, and the PCE of S7FAT devices become as large as 5.11% (~94.3% of control devices' PCE). We notice that the PCE of S1FAT devices is already at the 84% level of that of the control devices. Such observation indicates that FAT is a powerful low-temperature chemical reduction process, but that sufficient Pt-precursor supply is an essential prerequisite to fabricate SWCNT CEs having sufficient electrocatalytic capacity for triiodide reduction.

To elucidate the correlation between the Pt-precursor spin-coating numbers and the electrocatalytic capacity of FAT-SWCNT CEs, we conducted quantitative studies on Pt reduction based on EDS that can show atomic composition variations of the SWCNT CEs with respect to precursor spin-coating and FAT. Reduction of chloroplatinic acid precursor with formic acid proceeds according to the following chemical reaction:[31]

$$H_2PtCl_6 + 2HCOOH \rightarrow Pt + 6H^+ + 6Cl^- + CO_2(\uparrow)$$

Therefore, metallic Pt should appear concomitantly with the disappearance of chlorine after rinsing with ultrapure water. EDS measurements showed that FAT resulted in substantial decrease in chlorine contents from initial values of 7−8 wt % down to the final values of 0.3−0.8 wt % regardless of Pt-precursor spin-coating repetitions. However, the weight ratio between Pt and Cl was ~1.6 after a single spin-coating of chloroplatinic acid precursor and increased to 1.8−1.9 in response to Pt-precursor spin-coating more than 4 times. Presumably the increase in Pt/Cl ratio was indicative of

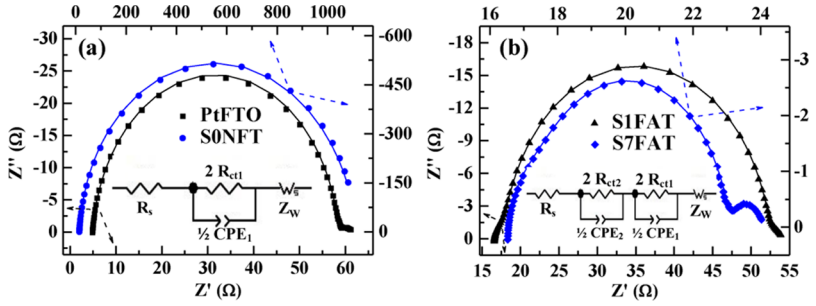

Figure 5. Nyquist plots of symmetric electrochemical cells consisting of two identical PtFTO (■), S0NFT (●), S1FAT (▲), and S7FAT (◆) counter electrodes. Solid lines are the best-fit curves according to the inset equivalent-circuit models of either one (a) or two (b) parallel combinations of charge-transfer resistor and constant phase elements in addition to a series resistance and Warburg impedance.

Table 2. Values of Equivalent Circuit Elements Correspond to the Best-Fit Curves in Figure 5

sample	R_s [a]	$R_{ct\text{-}1}$ [b]	$Z_{CPE\text{-}1}$ [b]		$R_{ct\text{-}2}$ [b]	$Z_{CPE\text{-}2}$ [b]		Z_W [c]	$C_{d\text{-}1}$ [d]	$\tau_{cal\text{-}1}$ [e]
ID	(Ω)	(Ω)	$Q_1 \times 10^5$	n_1	(Ω)	$Q_2 \times 10^5$	n_2	(Ω)	(μF)	(s)
PtFTO	4.91	26.7	2.65	0.943				2.36	17.0	4.54×10^{-4}
S0NFT	13.9	515	38.8	0.983				57.3	378	1.95×10^{-1}
S1FAT	16.6	17.2	36.6	0.946	0.62	20.4	0.972	1.46	275	4.73×10^{-3}
S7FAT	16.6	2.83	42.2	0.926	0.37	22.0	0.999	1.01	247	6.99×10^{-4}

[a] R_s is a series resistance. [b] $R_{ct\text{-}1}$ ($R_{ct\text{-}2}$) and $Z_{CPE\text{-}1}$ ($Z_{CPE\text{-}2}$) are charge transfer resistance and impedance of a constant phase element (CPE) corresponding to large (small) time constant. [c] Z_W is the Warburg impedance at 0.1 Hz. [d] $C_{d\text{-}i} = (Q_i R_{ct\text{-}i})^{1/n_i}/R_{ct\text{-}i}$ for $i = 1, 2$. [e] $\tau_{cal\text{-}i} = R_{ct\text{-}i}C_{d\text{-}i}$ for $i = 1, 2$.

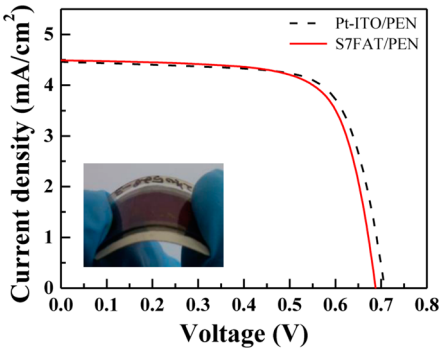

Figure 6. Comparison of photovoltaic performance of flexible DSSCs on PEN with different types of CEs. Solid (red) and dash (black) lines are $I-V$ curves of the flexible DSSCs with a Pt NP-SWCNT CE and a Pt-FTO CE, respectively.

inadvertent Pt reduction following multiple precursors spin-coating and drying at 85 °C. More dramatic increase in the Pt/Cl weight ratio was induced by FAT such that ratios of 13, 13, and 53 were noted for the respective spin-coating numbers of 1, 4, and 7. In particular, 7 repetitions of Pt-precursor spin-coating resulted in a very high Pt/Cl ratio after FAT. Nevertheless the PCE of S7FAT devices was not substantially increased compared to that of S4FAT devices. Arguably, not only the amount of reduced Pt but also the shape and size of metallic Pt are relevant to electrocatalytic capacity of FAT-SWCNT CEs. Additionally, Pt loading was quantified in terms of areal mass density by combining gravimetric measurements with EDS analysis results. For accurate gravimetric measurements extra SWCNT films with larger dimensions (area 6.25 ± 0.03 cm^2 and thickness 280 ± 22 nm) were prepared. Measurements with a microbalance (XP26, Mettler Toledo) showed a mass density of 42.5 ± 3.9 $\mu g/cm^2$ for such SWCNT films. To mimic the FAT-SWCNT CEs, the extra films were spin-coated with appropriate amounts of Pt-precursor solution and subsequently treated with formic acid. Both gravimetric and EDS measurements were carried out before and after FAT. To assess reliability of our analysis, we applied the same method to a SWCNT film decorated with e-beam evaporated Pt at a nominal thickness of 10 nm. The mass density of Pt loading we deduced from the combination of gravimetric and EDS measurements was 24.5 $\mu g/cm^2$, whereas the nominal Pt areal density in the calibration sample was estimated to be 21.5 $\mu g/cm^2$. This simple test proved the feasibility of Pt-loading quantification with an error of 10−15%.

Figure 3 shows the variation of Pt areal densities measured before and after FAT with respect to precursor spin-coating repetitions. The linearly increasing pre-FAT densities correspond mostly to elemental Pt in chloroplatinic acid precursors. However, the post-FAT densities represent metallic Pt particles because unreacted chloroplatinic acid precursors were thoroughly rinsed with ultrapure water before measurements. We note that the initial Pt density of 12.72 $\mu g/cm^2$ right after single Pt-precursor spin-coating was reduced down to 4.22 $\mu g/cm^2$ which is equivalent to a 33.2% retention of Pt as catalytic NPs. In comparison post-FAT Pt densities increased to 5.94 and 9.05 $\mu g/cm^2$ that were equivalent to the metallic Pt retention of 41.2 and 56.9% when the Pt-precursor solution was spin-coated 4 and 7 times, respectively. From the Pt quantification, we find that Pt-precursor spin coating and subsequent FAT are efficient way of making SWCNT-based CEs. For example, the PCE of S1FAT devices was about 84% of that of the control devices, whereas the metallic Pt loading in a SWCNT film spin-coated once with Pt precursor was less than 20% of that of a FTO CE coated with a nominally 10 nm thick Pt layer. Moreover, the PCE of S7FAT devices was 94.3% of control devices' PCE, in spite of their substantially smaller (only ∼40%) metallic Pt loading. Presumably the three-dimensional network morphology of entangled SWCNTs was advantageous for forming and attaching catalytically active Pt NPs. Smaller PCE difference between S7FAT and S4FAT devices in spite of 53% more Pt loading in the latter indicates that Pt density alone is not sufficient to account for the differences in PCE and that other factors such as size and spatial distributions of Pt NPs has to be considered.

The high-magnification SEM and TEM images in Figure 4 show that Pt NPs with a broad size distribution ranging from a few to tens of namometers in diameter were formed and decorating FAT-SWCNT CEs and SWCNTs themselves that consists of such CEs. We note that Pt NPs having tens of nanometers diameters were formed at the surface of a FAT-SWCNT CE in particular, whereas the SWCNTs including those at the interior of the three-dimensional network electrode were decorated with much smaller Pt NPs. Further study is required to elucidate the correlation between the size and spatial distributions of Pt NPs and the reduction capacity of FAT-SWCNT CEs.

Table 3. Average Solar-Cell Parameters of Two Types of Flexible DSSCs on PEN

sample ID [a]	V_{oc} (V)	J_{sc} (mA/cm^2)	fill factor (%)	PCE (%)
Pt-ITO/PEN	0.694 ± 0.011	4.31 ± 0.13	71.6 ± 1.4	2.14 ± 0.13
S7FAT/PEN	0.681 ± 0.005	4.41 ± 0.23	71.4 ± 0.9	2.14 ± 0.10

[a] CEs of these flexible DSSCs are either evaporated-Pt/ITO or Pt NP/SWCNT. Average values are estimated from three devices of each type.

For more quantitative comparison of catalytic activity for triiodide-ion reduction we performed EIS measurements on sandwich-type electrochemical cells that consisted of two identical CEs.[5,13,22] Such measurements on CE-only cells are useful to gain insights into the operation of CEs without extensive efforts to separate additional signals from other DSSC elements. As shown in Figure 5, the most dominant feature of Nyquist plots are semicircles that correspond to the time constants of 4.46×10^{-4}, 1.99×10^{-1}, 5.13×10^{-3}, and 6.34×10^{-4} s for PtFTO, S0NFT, S1FAT, and S7FAT CE, respectively. It is interesting to note that there is a strong correlation between the PCE values in Table 1 and the apparent time constants from the Nyquist plots; the smaller the time constant the larger PCE. The EIS spectra were fitted to equivalent circuit models that include series resistance R_s, which is mainly related to the sheet resistance of CEs, charge transfer resistance R_{ct}, constant phase element (CPE) Z_{CPE}, and Warburg impedance Z_W for electrolyte diffusion. Parallel R_{ct}-Z_{CPE} components represent electrochemical contributions of CE/electrolyte interfaces in terms of charge transfer for triiodide-ion reduction and double-layer capacitance. Interestingly, two R_{ct}-Z_{CPE} components were required to account for the EIS spectra of FAT-SWCNT CEs, whereas one component was sufficient for both Pt-FTO and SWCNT-only CEs. Arguably, two R_{ct}-Z_{CPE} components of FAT-SWCNT CEs indicate a bimodal distribution of catalytically active sites, and are consistent with the electron microscopy images in Figure 4 showing Pt NPs with diameter of either a few or tens of nanometers.

The values of equivalent-circuit elements corresponding to the best-fit curves in Figure 5 are summarized in Table 2. The CPE impedances Z_{CPE} is defined by two parameters Q and n as $Z_{CPE} = Q^{-1} (j\omega)^{-n}$. Using the fitting-produced Q and n values, we can deduce the value of double-layer capacitance from the relation $C_d = (QR_{ct})^{1/n}/R_{ct}$, and, can subsequently calculate time constants corresponding to triiodide-ion reduction: $\tau_{cal} = R_{ct}C_d$. The values of C_d and τ_{cal} are also listed in Table 2.

We note that R_s values of the two FAT-SWCNT CEs are almost identical, but larger than that of the SWCNT-only CE because of the dedoping effect (see Figure 1b). Comparison of PtFTO and S0NFT CEs shows that the charge transfer resistance of the SWCNT-only CE is 19.3 times larger than that of a conventional CE, which indicates much weaker electrocatalytic capacity of SWCNTs compared to Pt NPs. On the other hand, the double-layer capacitance of the SWCNT-only CE is 22.3 times larger than that of Pt NPs on a FTO glass because of network morphology of entangled SWCNTs. Random network structures of SWCNTs result in substantial increase in junction area with the electrolyte. Furthermore, it is harder for the electrolyte to diffuse thoroughly into network structures of entangled SWCNTs so that the Warburg impedance value of the SWCNT-only CE is 24.3 times larger than that of Pt NPs on an FTO glass. The two parallel R_{ct}-Z_{CPE} components of the FAT-SWCNT CEs represent two different time constants. For example, time constants for S1FAT of $\tau_{cal\text{-}1} = 4.73 \times 10^{-3}$ s and $\tau_{cal\text{-}2} = 9.73 \times 10^{-5}$ s were deduced from $R_{ct\text{-}1} = 17.2\ \Omega$ and $C_{d\text{-}1} = 275\ \mu$F, and $R_{ct\text{-}2} = 0.62\ \Omega$ and $C_{d\text{-}2} = 157\ \mu$F, respectively. Similarly for S7FAT, we deduced $\tau_{cal\text{-}1} = 6.99 \times 10^{-4}$ s and $\tau_{cal\text{-}2} = 7.99 \times 10^{-5}$ s from $R_{ct\text{-}1} = 2.83\ \Omega$ and $C_{d\text{-}1} = 275\ \mu$F, and $R_{ct\text{-}2} = 0.37\ \Omega$ and $C_{d\text{-}2} = 217\ \mu$F, respectively. It is plausible that the small time-constant R_{ct}-Z_{CPE} component represents the contribution of smaller Pt NPs which are only a few namometers in diameter and decorating individual SWCNTs. Furthermore, the large time-constant component corresponds to larger Pt NPs with diameter of tens of namometers, which reside mostly at the surfaces of FAT-SWCNT CEs. Arguably, the larger Pt NPs at the surface play a dominant role in reducing triiodide ions such that the PCE values show strong correlation with large time constants, and concomitantly Warburg-impedance values were substantially reduced. The smaller $R_{ct\text{-}1}$ and larger $C_{d\text{-}1}$ values of the FAT-SWCNT CEs compared to those of PtFTO indicate that the Pt NPs formed at the surfaces of SWCNT films by FAT are smaller than the sizes of Pt NPs at the FTO surface in a conventional CE. Extremely small values of $R_{ct\text{-}2}$ with reasonable size $C_{d\text{-}2}$ values suggests that with further studies on Pt-precursor preparation and FAT process, the size and spatial distributions of Pt NPs can be optimized to maximize electrocatalytic capacity of SWCNT CEs loaded with Pt NPs.

Figure 6 shows a representative $I-V$ curve of the first set of flexible DSSCs with a S7FAT CE on PEN. For comparison, an $I-V$ curve of a control flexible device with a more conventional evaporated Pt-ITO CE on PEN is shown together. These $I-V$ curves were measured with a mask of 0.235 cm^2. We note that there is no significant difference between the $I-V$ curves of the two types of flexible devise. As shown in Table 3, slightly smaller V_{OC} is compensated by slightly larger J_{SC} to result in almost identical PCEs. However, the PCE of the flexible DSSC with a S7FAT CE on PEN is only 42% of that of the DSSC with a S7FAT CE on glass. We argue that the use of thinner TiO_2 photoanode can account for most of the PCE loss. As long as porosity remains similar, the amount of dye loading is proportional to thicknesses of porous TiO_2 layers. The average thickness of a TiO_2 photoanode in flexible DSSCs, 6.09 ± 0.25 μm, is only 47% of that of other DSSCs on glass substrates. We expect that PCEs of flexible DSSCs with a Pt NP-SWCNT CE can be improved further with the optimization of device structure and fabrication process.

4. CONCLUSION

We developed a new type of CEs for DSSCs, which can be fabricated by exclusively using solution processes. Such solution-processed CEs are attractive because they are indispensable in developing flexible DSSCs, compatible with electronics-grade plastics, and suitable for large-scale production at low cost. The new CEs that are in essence semitransparent SWCNT electrodes decorated with Pt NPs were fabricated by combining a spin-coating process of aqueous SWCNT dispersion solution with a chemical reduction process that converts chloroplatinic acid precursor to Pt NPs by using formic acid as a reduction agent. Unlike other carbon-based CEs, the SWCNT-based CEs maintained optical transparency of 20−35% because thicknesses of ∼130 nm was sufficient to make surface resistance of SWCNT films comparable to those of FTO films. One major advantage of Pt NP-SWCNT CEs is the separation of the contribution of SWCNT films to charge transport from that of Pt NPs to catalytic activity for triiodide reduction. Therefore, catalytic capacity of Pt NP-SWCNT CEs can be improved further, in principle, without degrading the intrinsic merits of semitransparent SWCNT electrodes. In particular, fine controls of Pt-NP size distribution and density of Pt NPs at the surface of SWCNT electrodes are expected to make optimization of Pt NP-SWCNT CEs possible to result in performance superior to that of conventional Pt-FTO CEs.

■ ASSOCIATED CONTENT

Supporting Information

Change in transmittance and Raman spectra of Pt NP-SWCNT CEs following nitric- and formic-acid treatments. This material is available free of charge via the Internet at http://pubs.acs.org.

■ AUTHOR INFORMATION

Corresponding Author

*E-mail: soonil@ajou.ac.kr.

Notes

The authors declare no competing financial interest.

■ ACKNOWLEDGMENTS

This work was supported by the Technological Innovation R&D program (SA113679), which is funded by the Small and Medium Business Administration (SMBA, Korea), the Basic Science Research Program through the National Research Foundation of Korea (NRF), which is funded by the Ministry of Education (NRF-2009-0094046), and also by the National Research Foundation of Korea (NRF) Grant, which is funded by the Korea government (MEST) (No. NRF-2014R1A2A2A01005632)

■ REFERENCES

(1) Grätzel, M. Photoelectrochemical Cells. *Nature* **2001**, *414*, 338−344.

(2) Lungenschmied, C.; Dennler, G.; Neugebauer, H.; Sariciftci, S. N.; Glatthaar, M.; Meyer, T.; Meyer, A. Flexible, Long-lived, Large-area, Organic Solar Cells. *Sol. Energy Mater. Sol. Cells* **2007**, *91*, 379−384.

(3) Chirilua, A.; Buecheler, S.; Pianezzi, F.; Bloesch, P.; Gretener, C.; Uhl, A. R.; Fella, C.; Kranz, L.; Perrenoud, J.; Seyrling, S. Highly Efficient Cu (In, Ga) Se2 Solar Cells Grown on Flexible Polymer Films. *Nat. Mater.* **2011**, *10*, 857−861.

(4) Murakami, T. N.; Grätzel, M. Counter Electrodes for DSC: Application of Functional Materials as Catalysts. *Inorg. Chim. Acta* **2008**, *361*, 572−580.

(5) Fan, S.-Q.; Fang, B.; Kim, J. H.; Jeong, B.; Kim, C.; Yu, J.-S.; Ko, J. Ordered Multimodal Porous Carbon as Highly Efficient Counter Electrodes in Dye-Sensitized and Quantum-Dot Solar Cells. *Langmuir* **2010**, *26*, 13644−13649.

(6) Zhao, B.; Huang, H.; Jiang, P.; Zhao, H.; Huang, X.; Shen, P.; Wu, D.; Fu, R.; Tan, S. Flexible Counter Electrodes Based on Mesoporous Carbon Aerogel for High-Performance Dye-Sensitized Solar Cells. *J. Phys. Chem. C* **2011**, *115*, 22615−22621.

(7) Kang, D.-Y.; Lee, Y.; Cho, C.-Y.; Moon, J. H. Inverse Opal Carbons for Counter Electrode of Dye-Sensitized Solar Cells. *Langmuir* **2012**, *28*, 7033−7038.

(8) Hsieh, C.-K.; Tsai, M.-C.; Yen, M.-Y.; Su, C.-Y.; Chen, K.-F.; Ma, C.-C. M.; Chen, F.-R.; Tsai, C.-H. Direct Synthesis of Platelet Graphitic-Nanofibres as a Highly Porous Counter-Electrode in Dye-Sensitized Solar Cells. *Phys. Chem. Chem. Phys.* **2012**, *14*, 4058−4061.

(9) Roy-Mayhew, J. D.; Bozym, D. J.; Punckt, C.; Aksay, I. A. Functionalized Graphene as a Catalytic Counter Electrode in Dye-Sensitized Solar Cells. *ACS Nano* **2010**, *4*, 6203−6211.

(10) Koo, B.-K.; Lee, D.-Y.; Kim, H.-J.; Lee, W.-J.; Song, J.-S.; Kim, H.-J. Seasoning Effect of Dye-Sensitized Solar Cells with Different Counter Electrodes. *J. Electroceram.* **2006**, *17*, 79−82.

(11) Han, J.; Kim, H.; Kim, D. Y.; Jo, S. M.; Jang, S.-Y. Water-Soluble Polyelectrolyte-Grafted Multiwalled Carbon Nanotube Thin Films for Efficient Counter Electrode of Dye-Sensitized Solar Cells. *ACS Nano* **2010**, *4*, 3503−3509.

(12) Zhu, G.; Pan, L.; Lu, T.; Liu, X.; Lv, T.; Xu, T.; Sun, Z. Electrophoretic Deposition of Carbon Nanotubes Films as Counter Electrodes of Dye-Sensitized Solar Cells. *Electrochim. Acta* **2011**, *56*, 10288−10291.

(13) Lee, W. J.; Ramasamy, E.; Lee, D. Y.; Song, J. S. Efficient Dye-Sensitized Solar Cells with Catalytic Multiwall Carbon Nanotube Counter Electrodes. *ACS Appl. Mater. Interfaces* **2009**, *1*, 1145−1149.

(14) Zhang, D. W.; Li, X. D.; Chen, S.; Tao, F.; Sun, Z.; Yin, X. J.; Huang, S. M. Fabrication of Double-walled Carbon Nanotube Counter Electrodes for Dye-sensitized Solar Sells. *J. Solid State Electrochem.* **2010**, *14*, 1541−1546.

(15) Hao, F.; Dong, P.; Zhang, J.; Zhang, Y.; Loya, P. E.; Hauge, R. H.; Li, J.; Lou, J.; Lin, H. High Electrocatalytic Activity of Vertically Aligned Single-Walled Carbon Nanotubes Towards Sulfide Redox Shuttles. *Sci. Rep.* **2012**, *2*, No. 368.

(16) Cha, S. I.; Koo, B. K.; Seo, S. H.; Lee, D. Y. Pt-Free Transparent Counter Electrodes for Dye-Sensitized Solar Cells Prepared from Carbon Nanotube Micro-Balls. *J. Mater. Chem.* **2010**, *20*, 659−662.

(17) Liu, G.; Wang, H.; Li, X.; Rong, Y.; Ku, Z.; Xu, M.; Liu, L.; Hu, M.; Yang, Y.; Xiang, P. A Mesoscopic Platinized Graphite/Carbon Black Counter Electrode for a Highly Efficient Monolithic Dye-Sensitized Solar Cell. *Electrochim. Acta* **2012**, *69*, 334−339.

(18) Fan, B.; Mei, X.; Sun, K.; Ouyang, J. Conducting Polymer/Carbon Nanotube Composite as Counter Electrode of Dye-Sensitized Solar Cells. *Appl. Phys. Lett.* **2008**, *93*.

(19) Li, G.; Wang, F.; Jiang, Q.; Gao, X.; Shen, P. Carbon Nanotubes with Titanium Nitride as a Low-Cost Counter-Electrode Material for Dye-Sensitized Solar Cells. *Angew. Chem., Int. Ed.* **2010**, *49*, 3653−3656.

(20) Lin, J.-Y.; Liao, J.-H.; Hung, T.-Y. A Composite Counter Electrode of CoS/MWCNT with High Electrocatalytic Activity for Dye-Sensitized Solar Cells. *Electrochem. Commun.* **2011**, *13*, 977−980.

(21) Chen, H.-Y.; Liao, J.-Y.; Lei, B.-X.; Kuang, D.-B.; Fang, Y.; Su, C.-Y. Highly Catalytic Carbon Nanotube/Pt Nanohybrid-Based Transparent Counter Electrode for Efficient Dye-Sensitized Solar Cells. *Chem.—Asian J.* **2012**, *7*, 1795−1802.

(22) Kaniyoor, A.; Ramaprabhu, S. Enhanced Efficiency in Dye Sensitized Solar Cells with Nanostructured Pt Decorated Multiwalled Carbon Nanotube Based Counter Electrode. *Electrochim. Acta* **2012**, *72*, 199−206.

(23) Chu, H.; Shen, Y.; Lin, L.; Qin, X.; Feng, G.; Lin, Z.; Wang, J.; Liu, H.; Li, Y. Ionic-Liquid-Assisted Preparation of Carbon Nanotube-Supported Uniform Noble Metal Nanoparticles and Their Enhanced Catalytic Performance. *Adv. Funct. Mater.* **2010**, *20*, 3747−3752.

(24) Im, J. S.; Lee, S. K.; Yun, J.; Lee, Y.-S. CNT−Pt Counter Electrode Prepared Using a Polyol Process to Achieve High Performance in Dye-Sensitised Solar Cells. *J. Ind. Eng. Chem.* **2012**, *18*, 1023−1028.

(25) Chang, L.-Y.; Lee, C.-P.; Huang, K.-C.; Wang, Y.-C.; Yeh, M.-H.; Lin, J.-J.; Ho, K.-C. Facile Fabrication of PtNP/MWCNT Nanohybrid Films for Flexible Counter Electrode in Dye-Sensitized Solar Cells. *J. Mater. Chem.* **2012**, *22*, 3185−3191.

(26) Huang, K.-C.; Wang, Y.-C.; Chen, P.-Y.; Lai, Y.-H.; Huang, J.-H.; Chen, Y.-H.; Dong, R.-X.; Chu, C.-W.; Lin, J.-J.; Ho, K.-C. High Performance Dye-Sensitized Solar Cells Based on Platinum Nanoparticle/Multi-Wall Carbon Nanotube Counter Electrodes: The Role of Annealing. *J. Power Sources* **2012**, *203*, 274−281.

(27) Kim, S. J.; Park, Y. J.; Ra, E. J.; Kim, K. K.; An, K. H.; Lee, Y. H.; Choi, J. Y.; Park, C. H.; Doo, S. K.; Park, M. H. Defect-Induced Loading of Pt Nanoparticles on Carbon Nanotubes. *Appl. Phys. Lett.* **2007**, *90*.

(28) Liu, C.-T.; Wang, Y.-C.; Dong, R.-X.; Wang, C.-C.; Huang, K.-C.; Vittal, R.; Ho, K.-C.; Lin, J.-J. A Dual-Functional Pt/CNT TCO-Free Counter Electrode for Dye-Sensitized Solar Cell. *J. Mater. Chem.* **2012**, *22*, 25311−25315.

(29) KumaráMulmudi, H.; KumaráBatabyal, S.; MingáLam, Y.; GautamáMhaisalkar, S. Metal/Metal Sulfide Functionalized Single-Walled Carbon Nanotubes: FTO-Free Counter Electrodes for Dye Sensitized Solar Cells. *Phys. Chem. Chem. Phys.* **2012**, *14*, 9906−9911.

(30) Chen, L.; Tan, W.; Zhang, J.; Zhou, X.; Zhang, X.; Lin, Y. Fabrication of High Performance Pt Counter Electrodes on Conductive Plastic Substrate for Flexible Dye-Sensitized Solar Cells. *Electrochim. Acta* **2010**, *55*, 3721−3726.

(31) Yang, D.-Q.; Sun, S.; Dodelet, J.-P.; Sacher, E. A Facile Route for the Self-Organized High-Density Decoration of Pt Nanoparticles on Carbon Nanotubes. *J. Phys. Chem. C* **2008**, *112*, 11717−11721.
(32) Matoh, L.; Škofic, I. K.; Čeh, M.; Bukovec, N. A Novel Method for Preparation of a Platinum Catalyst at Low Temperatures. *J. Mater. Chem.* **2013**, *1*, 1065−1069.
(33) Kim, S.; Yim, J.; Wang, X.; Bradley, D. D.; Lee, S.; deMello, J. C. Spin-and Spray-Deposited Single-Walled Carbon-Nanotube Electrodes for Organic Solar Cells. *Adv. Funct. Mater.* **2010**, *20*, 2310−2316.
(34) Park, J.; Koo, H.-J.; Yoo, B.; Yoo, K.; Kim, K.; Choi, W.; Park, N.-G. On the I−V Measurement of Dye-Sensitized Solar Cell: Effect of Cell Geometry on Photovoltaic Parameters. *Sol. Energy Mater. Sol. Cells* **2007**, *91*, 1749−1754.
(35) Yim, J. H.; Kim, Y. S.; Koh, K. H.; Lee, S. Fabrication of Transparent Single Wall Carbon Nanotube Films with Low Sheet Resistance. *J. Vac. Sci. Technol., B* **2008**, *26*, 851−855.